frontiers in Materials

ORIGINAL RESEARCH
published: 12 January 2022
doi: 10.3389/fmats.2021.821126

Effect of the Addition of 4wt% Zr to BCC Solid Solution $Ti_{52}V_{12}Cr_{36}$ at Melting/Milling on Hydrogen Sorption Properties

Amol Kamble[1]*, *Pratibha Sharma*[2] and *Jacques Huot*[3]

[1]Department of Mechanical Engineering, Amity School of Engineering and Technology, Amity University Mumbai, Maharashtra, India, [2]Department of Energy Science and Engineering, IIT Bombay, Mumbai, India, [3]IRH, Université du Québec à Trois-Rivières, Trois-Rivières, QC, Canada

The addition of 4 wt% Zr to $Ti_{52}V_{12}Cr_{36}$ alloy was carried out in two different ways: arc-melting or ball-milling. The cast alloy showed rapid hydrogen absorption up to 3.6 wt% of hydrogen capacity within 15 min. Ball milling this sample worsened the kinetics, and no hydrogen absorption was registered when milling was carried out for 30 or 60 min. When zirconium is added by ball-milling, the kinetic is slower than that when addition is by arc-melting. This is due to the fact that when added by milling, zirconium does not form a ternary phase with Ti, V, and Cr but instead is just dispersed on the particles' surface.

Keywords: hydrogen storage, mechanical alloying, Ti-based metal hydrides, Zr-addition, ball milling

OPEN ACCESS

Edited by:
Xiubo Xie,
Yantai University, China

Reviewed by:
Huai-Jun Lin,
Jinan University, China
Guoling Li,
Qingdao University, China

***Correspondence:**
Amol Kamble
amul.kamble@gmail.com

Specialty section:
This article was submitted to Energy Materials, a section of the journal Frontiers in Materials

Received: *23 November 2021*
Accepted: *20 December 2021*
Published: *12 January 2022*

Citation:
Kamble A, Sharma P and Huot J (2022) Effect of the Addition of 4 wt% Zr to BCC Solid Solution $Ti_{52}V_{12}Cr_{36}$ at Melting/Milling on Hydrogen Sorption Properties. Front. Mater. 8:821126. doi: 10.3389/fmats.2021.821126

INTRODUCTION

Hydrogen has a great potential to become a clean energy carrier but needs development in terms of its production, safety, storage, and transport (Sakintuna et al., 2007; Modi and Aguey, 2021). For hydrogen storage applications, metal hydrides have the advantage of a high-volumetric capacity at low hydrogen pressure. Body-centered cubic (BCC) solid solution metal hydrides have relatively high-gravimetric hydrogen capacity of around 3.5 wt% at room temperature under low hydrogen pressure (2–3 MPa) (Kabutomori et al., 1995; Akiba and Iba, 1998; Sakintuna et al., 2007; Liu et al., 2009; Miraglia et al., 2012; Bibienne et al., 2014; Bibienne et al., 2015; Kamble et al., 2017; Kamble et al., 2018; Modi and Aguey, 2021). However, they usually form very stable monohydrides which makes the reversible practical capacity only half of the total capacity (Akiba and Iba, 1998; Bibienne et al., 2014; Bibienne et al., 2015; Kamble et al., 2017).

TiVCr and TiVMn are well-studied BCC alloys which show a total hydrogen absorption of around 3.6 wt% (Miraglia et al., 2012; Bibienne et al., 2015; Kamble et al., 2017; Kamble et al., 2018). One problem of these alloys is that the first hydrogenation, the so-called activation, shows a long incubation time which makes the hydrogenation difficult and time-consuming (Miraglia et al., 2012; Bibienne et al., 2015). The alloys have to be subjected to high temperature and pressure, and a few hydrogenation/dehydrogenation cycles have to be performed before the alloy could fully absorb hydrogen. Elimination of the incubation time could greatly improve the first hydrogenation process. The activation process is still not well understood, but it can be improved by many means such as introduction of additives/catalysts, method of synthesis, or heat treatments (Huot, 2012; Miraglia et al., 2012; Bibienne et al., 2015; Banerjee et al., 2016; Young et al., 2016; Balcerzak, 2017; Kamble et al., 2017).

Additives could introduce secondary phases which help the first hydrogenation (Miraglia et al., 2012; Bibienne et al., 2015; Kamble et al., 2017). Skryabina et al. (Skryabina et al., 2016) melted $(TiCr_{1.8})_{100-x}V_x$ for x = 20, 40, 60, and 80 with 4 mol% Zr_7Ni_{10} and reported the dependence of

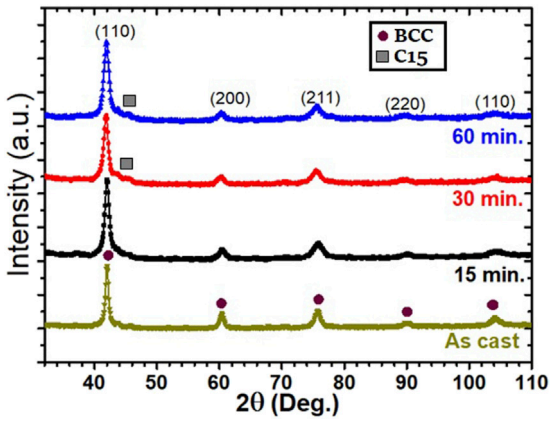

FIGURE 1 | XRD patterns of cast BCC $Ti_{52}V_{12}Cr_{36}$ + 4 wt% Zr and milled for 15, 30, and 60 min.

hydrogen uptake, reversible hydrogen capacity and desorption temperature on the vanadium content, and dependence upon melted with the Zr–Ni additive. Miraglia et al. (Kamble et al., 2017) found dramatic improvement in activation when 4 wt% Zr_7Ni_{10} was added to BCC $Ti_{33}V_{30}Cr_{37}$ alloy by induction melting.

Ball milling is a well-known technique used for getting nanocrystallinity, modifying surfaces, and producing alloys by mechanical alloying (Hu et al., 2004; Danaie et al., 2011; Huot, 2012). The reduced crystallite size and increase in defect density induced by the severe plastic deformation techniques could facilitate quick hydrogen absorption (Huot, 2012). M. Balcerzak (Balcerzak, 2017) used mechanical alloying to synthesize $Ti_{2-x}V_x$ (x = 0.5, 0.75, 1, 1.25, 1.5). They reported the formation of nanocrystalline BCC phase alloys after 14 h of milling. Alloys with high proportion of Ti had higher hydrogen capacity. X. B. Yu et al. (Yu et al., 2005) added 10wt% nanoparticles of $LaNi_{3.75}Co_{0.75}Mn_{0.4}Al_{0.3}$ to quenched $Ti_{47}V_{28}Mn_{15}Cr_{10}$ by ball-milling. The layer of nanoparticles modifies the surface of the pristine alloy. The nanoparticles acted as gateways for hydrogen atoms to enter into the bulk of alloy resulting in an improvement in activation.

In a previous investigation, we showed that as-cast of $Ti_{52}V_{12}Cr_{36}$ + 4 wt% Zr_7Ni_{10} has fast first hydrogenation at room temperature under 2 MPa of hydrogen. This was attributed to a Zr–Ni-rich secondary phase (Bibienne et al., 2014). The relative impact of zirconium and nickel as an additive on first hydrogenation was investigated, and it was found that addition of zirconium is more beneficial than that of nickel (Kamble et al., 2018). The relative effect of the additive and particle size on hydrogen sorption of BCC $Ti_{52}V_{12}Cr_{36}$ + 4 wt % Zr showed that the chemical composition has more influence on hydrogenation behavior than particle size (Miraglia et al., 2012). Ball milling is an energetic way to get nanocrystalline structures and high defect density. This may lead to quick hydrogen interaction. Thus, adding zirconium by milling will tightly bind the BCC and zirconium particle, and this may act as gateways for quick hydrogen absorption. In this article, we present an investigation on the use of ball-milling for adding zirconium to a BCC alloy and also for obtaining a nanocrystalline structure.

ARTICLE TYPES

Tier 1: Brief Research Report, B-type Article

MATERIALS AND METHODS

The raw materials titanium (sponge, 3–19 mm, 99.95%), vanadium (granules, 1–3 mm, 99.7%), chromium (pieces, irregular, 99%), and zirconium (sponge, 0.8–25.4 mm, 99.5%) were purchased from Alfa Aesar and melted in the required stoichiometry. Two compositions were melted: $Ti_{52}V_{12}Cr_{36}$ and $Ti_{52}V_{12}Cr_{36}$ + 4 wt% Zr. The melting was carried out under argon atmosphere using an arc-melting apparatus from Centorr Associates Inc, NH, United States. Each composition was melted three times by flipping the pellet each time in order to achieve homogeneity.

To avoid oxidation, the sample pellets were crushed into powder using a mortar and pestle inside an argon-filled glove box. The crushed powders were put inside a hardened steel ball-milling vial with a powder to ball ratio of 10:1. Ball milling was performed using a Spex 8000 apparatus. For Zr addition at melting, the as-cast $Ti_{52}V_{12}Cr_{36}$ + 4 wt% Zr was milled for 15, 30, and 60 min. Milling for the same periods was also carried out on the as-cast $Ti_{52}V_{12}Cr_{36}$ to which 4 wt % of zirconium was added at milling. Scanning electron microscopy was performed using a JEOL scanning electron microscope JSM-5500 with an attachment for energy

TABLE 1 | Refinement of cast $Ti_{52}V_{12}Cr_{36}$ + 4 wt% Zr milled for 15, 30, and 60 min. The error on the last significant digit is indicated by the number in parentheses.

Sample	Phase	Abundance (%)	a (Å)	Crystallite size (nm)	Microstrain (%)
As-cast with Zr	BCC	100	3.1116 (7)	10.3 (2)	
(As-cast with Zr) Milled for 15 min	BCC	100	3.105 (4)	7.6 (4)	0.19 (2)
(As-cast with Zr) Milled for 30 min	BCC	87 (1)	3.113 (1)	8.3 (2)	0.23 (1)
	C15	13 (1)	7.003 (3)	8.9 (1)	
(As-cast with Zr) Milled for 60 min	BCC	88 (1)	3.116 (1)	7.6 (2)	0.27 (1)
	C15	12 (1)	6.993 (3)	8.9 (1)	

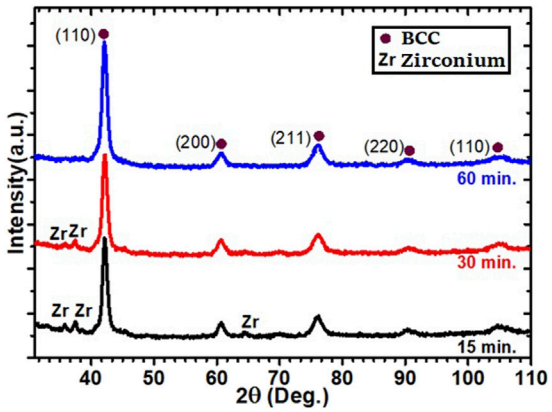

FIGURE 2 | XRD patterns of cast BCC $Ti_{52}V_{12}Cr_{36}$ milled with 4 wt% Zr for 15, 30, and 60 min.

dispersive spectroscopy (EDS) to measure the chemical composition.

The first hydrogenation was measured at 298 K under 20 bars hydrogen pressure using a homemade hydrogen titration system. X-ray diffraction (XRD) patterns were taken on a D8 Focus Bruker X-ray powder diffractometer with Cu Kα radiation. The XRD patterns were analyzed by Rietveld refinement using TOPAS software in order to determine the crystal structure parameters such as lattice parameters and crystallite size (Cheary et al., 2004; Robert et al., 2018).

RESULTS AND DISCUSSION

X-Ray Diffraction

The XRD pattern of as-cast BCC $Ti_{52}V_{12}Cr_{36}$ with the additive 4 wt% Zr has been shown in our previous report (Kamble et al., 2018). It presents a single phase BCC crystal structure (S. G.- Im-3m). The diffraction patterns of the milled samples are similar to those of the unmilled ones as shown in **Figure 1**. There is no indication of the creation of a new phase upon milling. The peak broadening with milling time indicates reduction in crystallite size and presence of microstrains.

Rietveld refinement was carried out on each pattern, and the results are tabulated in **Table 1**. The refinement results for the alloy with 4 wt% Zr are from the previous research work and are merged in **Table 1** for comparison (Kamble et al., 2018). **Table 1** shows that there is no influence of ball-milling on the lattice parameter but a reduction in crystallite size. When milling is performed for 30 and 60 min, there is an appearance of a C15 type Laves phase.

In another set of experiments, zirconium was added by ball-milling. The alloy $Ti_{52}V_{12}Cr_{36}$ was first arc-melted and thereafter ball-milled with 4 wt% Zr. The XRD patterns of the material after different milling times are presented in **Figure 2**.

In case of Zr-addition at milling, all samples exhibit the main BCC crystal structure with small minor peaks of zirconium. These peaks diminish with milling time, which may indicate a reduction of Zr crystallite size.

The results of the Rietveld refinement for zirconium addition by milling are shown in **Table 2**. The refinement results for the cast of alloy without 4 wt% Zr are from the previous research work and are merged in **Table 2** for comparison (Kamble et al., 2018).

The lattice parameter of the BCC phase does not change with milling time. For the zirconium, the lattice parameters seem to decrease with milling time, but we have to point out that the error is also increasing with milling time. This is because the peak intensities are greatly reduced, and thus the exact location of the peak's maximum is difficult to measure. The reduction of peak maximum is due to the reduction of crystallite size as seen in **Table 2**. We see that, with milling time, the crystallite size of BCC and zirconium converge toward similar values. Moreover, the value of the crystallite size and microstrain for the BCC phase is similar to the values reported in **Table 1**. We could conclude that the effectiveness of ball-milling is the same for Zr added at melting or at milling.

First Hydrogenation

The effect of milling on the first hydrogenation of as-cast $Ti_{52}V_{12}Cr_{36}$ + 4 wt% Zr alloy is shown in **Figure 3**. As a reference, the first hydrogenation curve of the as-cast alloy presented in ref (Kamble et al., 2018) is included.

We see that the incubation time is quite long but thereafter the kinetic is fast. In previous investigations, it was found that the fast kinetic could be attributed to a network of the Zr-rich secondary phase that acts as gateways for hydrogen (Bibienne et al., 2014; Kamble et al., 2017). Milling for 15 min decreases the incubation time, but the final capacity is reduced as well as slower kinetics.

TABLE 2 | Refinement of cast $Ti_{52}V_{12}Cr_{36}$ milled with 4 wt% Zr for 15, 30, and 60 min. The error on the last significant digit is indicated by the number in parentheses.

Sample	Phase	Abundance (wt%)	Lattice parameter (Å)	Crystallite size (nm)	Microstrain (%)
As-cast	BCC	100	a = 3.107 (3)	19.8 (8)	
$Ti_{52}V_{12}Cr_{36}$ ball-milled for 15 min with Zr	BCC	95.1 (5)	a = 3.0990 (9)	10.6 (4)	0.29 (1)
	Zirconium (HCP)	4.9 (5)	a = 3.236 (2)	21 (7)	0.16 (5)
			c = 5.156 (7)		
$Ti_{52}V_{12}Cr_{36}$ ball-milled for 30 min with Zr	BCC	97.9 (2)	a = 3.095 (1)	8.4 (3)	0.26 (1)
	Zirconium (HCP)	2.1 (2)	a = 3.234 (4)	7 (1)	
			c = 5.15 (1)		
$Ti_{52}V_{12}Cr_{36}$ ball-milled for 60 min with Zr	BCC	100	a = 3.095 (1)	9.0 (2)	0.30 (1)

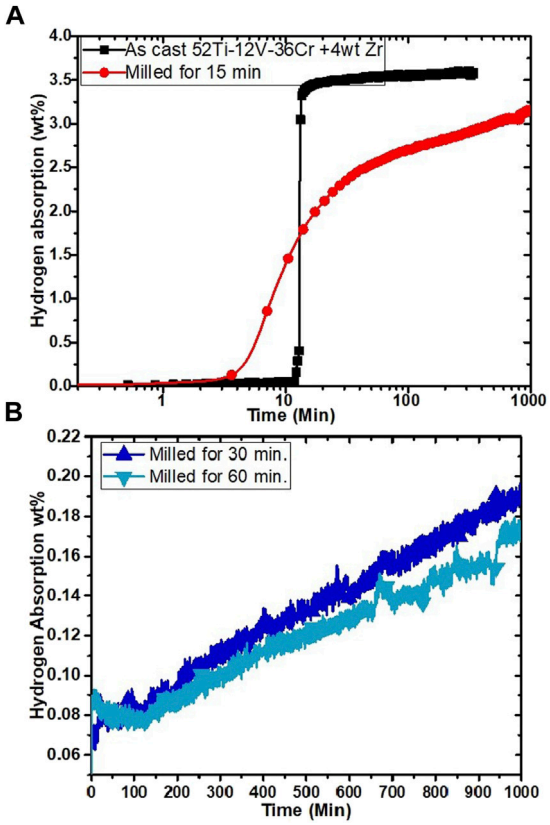

FIGURE 3 | First hydrogenation curves: as-cast $Ti_{52}V_{12}Cr_{36}$ + 4 wt% Zr and milled for 15 min **(A)** and milled for 30 and 60 min **(B)**.

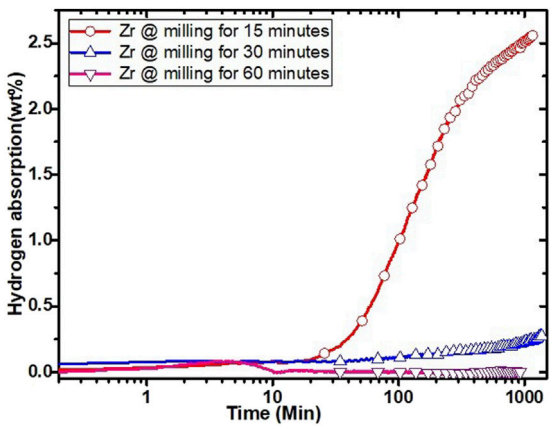

FIGURE 4 | First hydrogenation curves of as-cast $Ti_{52}V_{12}Cr_{36}$ milled for 15, 30, and 60 min with 4 wt% Zr.

Further milling for 30 or 60 min (**Figure 3B**) effectively makes the alloy inert to hydrogen. The reason for such behavior is unclear. It is known that reduction of crystallite size may bring a smaller capacity due to the higher proportion of grain boundaries (Lv et al., 2019). However, in the present case the reduction of capacity is too important to be only attributed to the reduction of crystallite size.

In a previous investigation, it was shown that the bare alloy $Ti_{52}V_{12}Cr_{36}$ could absorb 3.6 wt% of hydrogen at room temperature and under 20 bars of hydrogen but only after 22 h of incubation time (Kamble et al., 2017). **Figure 4** shows the first hydrogenation curves for samples where Zr was added by milling. It shows that the sample milled for 15 min could absorb hydrogen but at a slower rate and longer incubation time than the sample in which Zr is directly added in melting (**Figure 3**). The full capacity was not reached because the absorption was terminated after 1,000 min. Further milling for 30 and 60 min makes the sample inert to hydrogen.

Scanning Electron Microscopy

As only the samples milled for 15 min showed absorption in both methods of Zr addition, they were studied further. **Figure 5** shows the BSE image of both samples after milling.

For the as-cast $Ti_{52}V_{12}Cr_{36}$ + 4 wt% Zr milled for 15 min, the particles show a uniform gray shade. This indicates uniform distribution of the elements. A previous investigation showed that there is a zirconium-rich secondary phase in this alloy (Kamble et al., 2018). However, at the scale of **Figure 5** and with an unpolished sample, this secondary phase is not visible. In the case of as-cast $Ti_{52}V_{12}Cr_{36}$ milled with 4 wt% Zr, the particles show bright areas which most likely are zirconium particles. To verify this, we performed EDS analysis on both samples.

Energy Dispersive Spectroscopy

For both samples, the bulk composition was measured by recording the EDS spectrum over the whole field of view under low magnification. The bulk-measured composition agreed with the nominal composition for both samples.

To check the nature of the bright areas in **Figure 5B**, an elemental mapping was performed and is presented in **Figure 6**.

It is clear that Ti, V, and Cr elements are evenly distributed, and zirconium is in small particles attached to the BCC alloy. It thus confirms the results of X-ray diffraction that the addition of zirconium by ball-milling results in small particles of zirconium bonded to BCC particles and no alloying with the bulk to form a Zr-rich alloy as seen in the arc-melted alloy (Kamble et al., 2017; Kamble et al., 2018). This indicates that the milling duration of 15 min is too small to produce a Zr-rich secondary phase.

X-Ray Diffraction After Hydrogenation

The X-ray diffraction of hydrogenated samples was registered in order to see the hydrogenated crystal structure. The respective XRD patterns are shown in **Figure 7**. For as-cast samples, the BCC crystal structure turns into the FCC crystal structure upon hydrogenation (**Figure 7A**). This confirms the formation of a di-hydride phase. For the as-cast $Ti_{52}V_{12}Cr_{36}$ + 4 wt% Zr further

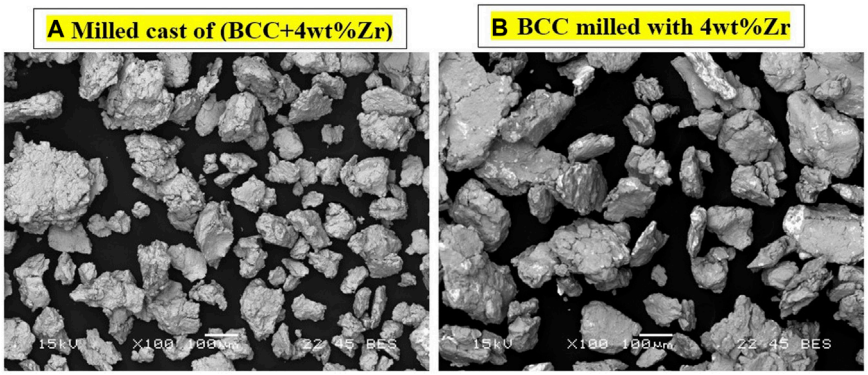

FIGURE 5 | BSE images of as-cast $Ti_{52}V_{12}Cr_{36}$ + 4 wt% Zr **(A)** and cast $Ti_{52}V_{12}Cr_{36}$ with 4 wt% Zr **(B)** both milled for 15 min.

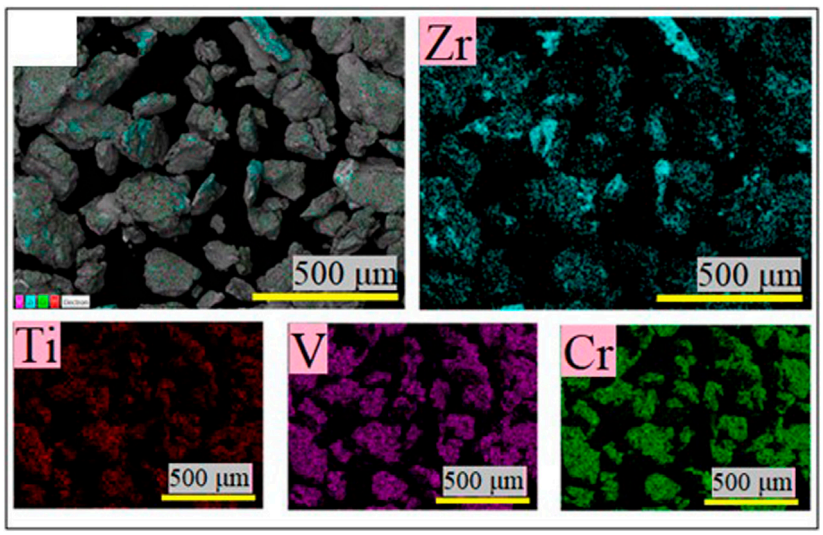

FIGURE 6 | Elemental mapping of BCC $Ti_{52}V_{12}Cr_{36}$ milled with 4 wt% Zr for 15 min.

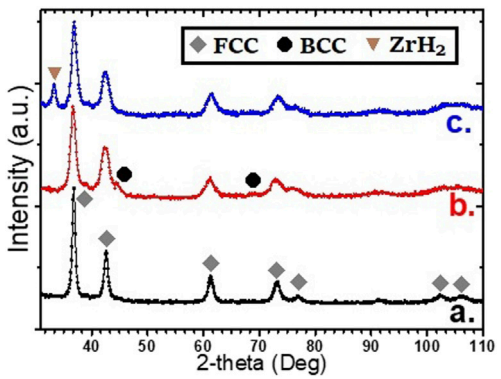

FIGURE 7 | XRD curves upon hydrogenation of as-cast $Ti_{52}V_{12}Cr_{36}$ + 4 wt% Zr **(A)**, milled for 15 min **(B)**, and cast $Ti_{52}V_{12}Cr_{36}$ milled for 15 min with 4 wt% Zr **(C)**.

milled for 15 min (**Figure 7B**), the pattern also shows an FCC phase, but the peaks are broader. This is due to the smaller crystallite size of the BCC phase of the ball-milled sample as reported in **Table 1**.

In the case of the $Ti_{52}V_{12}Cr_{36}$ milled with Zr (**Figure 7C**), the pattern shows an FCC phase but also the presence of a ZrH_2 phase. This is understandable as free Zr was identified in this sample after milling, and ZrH_2 is a very stable hydride.

In **Table 3**, the lattice parameters and crystallite size of the FCC phase as determined by Rietveld refinement are listed. We see that the crystallite size of the FCC phase in the hydrided samples is slightly larger than that of the BCC phase in the corresponding as-cast or as-milled samples. This is expected as hydrogenation usually results in a swelling of the unit cell due to the inclusion of hydrogen atoms in the lattice.

TABLE 3 | Refinement of cast $Ti_{52}V_{12}Cr_{36}$ + 4 wt% Zr milled for 15, 30, and 60 min. The error on the last significant digit is indicated by the number in parentheses.

Sample	Phase	Abundance (wt%)	Lattice parameter (Å)	Crystallite size (nm)	Microtrain (%)
As-cast with Zr	FCC	100	4.3445 (7)	14.2 (4)	0.262 (6)
As-cast with Zr and milled for 15 min	BCC	30 (2)	3.090 (4)	1.23 (9)	
	FCC	70 (2)	4.358 (2)	9.1 (5)	0.52 (2)
As-cast and milled for 15 min with Zr	BCC	18 (1)	3.112 (2)	3.6 (3)	
	FCC	74 (1)	4.331 (2)	11.0 (6)	0.52 (1)
	ZrH_2	7.4 (4)	a: 3.443 (3)	7.5 (5)	
			c: 4.670 (6)		

CONCLUSION

The addition of Zr at milling and at melting was investigated. In the case of addition of Zr at melting, the alloy shows only the BCC crystal structure. A C15 phase is produced upon further milling for 30 and 60 min. In the case of Zr addition at milling, there are some peaks of Zr along with the BCC structure, but no alloying is observed. The addition of Zr by milling leads to heterogenous presence of Zr on the surface of BCC particles. Thus, we were able to test the effect of pure zirconium on the hydrogen sorption behavior of the $Ti_{52}V_{12}Cr_{36}$ alloy.

The ball-milling adversely reduces kinetics and hydrogen capacity for both ways to add zirconium. In fact, milling for more than 15 min makes the samples inert to hydrogen. The change in hydrogenation behavior upon ball-milling of the alloy with the additive remains unexplainable. The first hydrogenation of BCC alloys without the additive has been reported to be very difficult (Bibienne et al., 2014; Kamble et al., 2017). Milling this alloy with 4 wt% Zr for 15 min makes hydrogenation possible but at a slow rate and with reduced hydrogen capacity. The reason for the poor performance of the alloys with Zr added by milling may be due to the fact that milling does not produce a Zr-rich secondary phase. Therefore, the addition of Zr is optimum when carried out at casting. Ball milling is not suitable for adding Zr to BCC alloys for the purpose of getting fast first hydrogenation.

DATA AVAILABILITY STATEMENT

The original contributions presented in the study are included in the article/Supplementary Material; further inquiries can be directed to the corresponding author.

AUTHOR CONTRIBUTIONS

AK has carried out the experimental work and wrote the article as the first and corresponding author. PS has supervised the work and mentored. JH has supervised the experimental work and reviewed the article.

FUNDING

The Queen Elizabeth II Diamond Jubilee Scholarship supported the stay of AK at the University Du Quebec Trois-Rivieres (UQTR), Canada, for his doctoral student exchange program, when the experiments were performed at the Institute of Hydrogen (IRH), UQTR, TR, QC, Canada.

ACKNOWLEDGMENTS

AK would like to thank the Queen Elizabeth II Diamond Jubilee Scholarship for PhD fellowship. AK is appreciative to Amity School of Engineering and Technology, Amity University Mumbai, MH, India, for its professional support.

REFERENCES

Akiba, E., and Iba, H. (1998). Hydrogen Absorption by Laves Phase Related BCC Solid Solution. *Intermetallics* 6, 461–470. doi:10.1016/S0966-9795(97)00088-5

Balcerzak, M. (2017). Structure and Hydrogen Storage Properties of Mechanically Alloyed Ti-V Alloys. *Int. J. Hydrogen Energ.* 42, 23698–23707. doi:10.1016/j.ijhydene.2017.03.224

Banerjee, S., Kumar, A., Ruz, P., and Sengupta, P. (2016). Influence of Laves Phase on Microstructure and Hydrogen Storage Properties of Ti-Cr-V Based alloy. *Int. J. Hydrogen Energ.* 41, 18130–18140. doi:10.1016/j.ijhydene.2016.07.088

Bibienne, T., Bobet, J.-L., and Huot, J. (2014). Crystal Structure and Hydrogen Storage Properties of Body Centered Cubic 52Ti-12V-36Cr alloy Doped with Zr_7Ni_{10}. *J. Alloys Compd.* 607, 251–257. doi:10.1016/j.jallcom.2014.04.062

Bibienne, T., Razafindramanana, V., Bobet, J.-L., and Huot, J. (2015). Synthesis, Characterization and Hydrogen Sorption Properties of a Body Centered Cubic 42Ti-21V-37Cr alloy Doped with Zr_7Ni_{10}. *J. Alloys Compd.* 620, 101–108. doi:10.1016/j.jallcom.2014.08.156

Cheary, R. W., Coelho, A. A., and Cline, J. P. (2004). Fundamental Parameters Line Profile Fitting in Laboratory Diffractometers. *J. Res. Natl. Inst. Stand. Technol.* 109, 1. doi:10.6028/jres.109.002

Danaie, M., Mauer, C., Mitlin, D., and Huot, J. (2011). Hydrogen Storage in Bulk Mg-Ti and Mg-Stainless Steel Multilayer Composites Synthesized via Accumulative Roll-Bonding (ARB). *Int. J. Hydrogen Energ.* 36, 3022–3036. doi:10.1016/j.ijhydene.2010.12.006

Hu, Y. Q., Zhang, H. F., Yan, C., Ye, L., Ding, B. Z., and Hu, Z. Q. (2004). Preparation and Hydrogenation of Body-Centered-Cubic $TiCr_2$ alloy. *Mater. Lett.* 58, 783–786. doi:10.1016/j.matlet.2003.07.011

Huot, J. (2012). Nanocrystalline Metal Hydrides Obtained by Severe Plastic Deformations. *Metals* 2, 22–40. doi:10.3390/met2010022

Kabutomori, T., Takeda, H., Wakisaka, Y., and Ohnishi, K. (1995). Hydrogen Absorption Properties of TiCrA (A ≡ V, Mo or Other Transition Metal) B.C.C. Solid Solution Alloys. *J. Alloys Compd.* 231, 528–532. doi:10.1016/0925-8388(95)01859-X

Kamble, A., Sharma, P., and Huot, J. (2017). Effect of Doping and Particle Size on Hydrogen Absorption Properties of BCC Solid Solution 52Ti-12V-36Cr. *Int. J. Hydrogen Energ.* 42, 11523–11527. doi:10.1016/j.ijhydene.2017.02.137

Kamble, A., Sharma, P., and Huot, J. (2018). Effect of Addition of Zr, Ni, and Zr-Ni alloy on the Hydrogen Absorption of Body Centred Cubic 52Ti-12V-36Cr alloy. *Int. J. Hydrogen Energ.* 43, 7424–7429. doi:10.1016/j.ijhydene.2018.02.106

Liu, X., Jiang, L., Li, Z., Huang, Z., and Wang, S. (2009). Improve Plateau Property of $Ti_{32}Cr_{46}V_{22}$ BCC alloy with Heat Treatment and Ce Additive. *J. Alloys Compd.* 471, L36–L38. doi:10.1016/j.jallcom.2008.04.004

Lv, P., Guzik, M. N., Sartori, S., and Huot, J. (2019). Effect of ball Milling and Cryomilling on the Microstructure and First Hydrogenation Properties of TiFe+4wt.% Zr alloy. *J. Mater. Res. Technol.* 8, 1828–1834. doi:10.1016/j.jmrt.2018.12.013

Miraglia, S., de Rango, P., Rivoirard, S., Fruchart, D., Charbonnier, J., and Skryabina, N. (2012). Hydrogen Sorption Properties of Compounds Based on BCC $Ti_{1-x}V_{1-y}Cr_{1+x+y}$ Alloys. *J. Alloys Compd.* 536, 1–6. doi:10.1016/j.jallcom.2012.05.008

Modi, P., and Aguey, Z-K-F. (2021). Room Temperature Metal Hydrides for Stationary and Heat Storage Applications: A Review. *Front. Energ. Res.* 9, 128–152. doi:10.3389/fenrg.2021.616115

Robert, E. D., Andreas, L., and John, S. O. E. (2018). *Rietveld Refinement*. Berlin, Boston: De Gruyter. doi:10.1515/9783110461381

Sakintuna, B., Lamaridarkrim, F., and Hirscher, M. (2007). Metal Hydride Materials for Solid Hydrogen Storage: A Review☆. *Int. J. Hydrogen Energ.* 32, 1121–1140. doi:10.1016/j.ijhydene.2006.11.022

Skryabina, N. E., Fruchart, D., Fruchart, D., Medvedeva, N. A., De Rango, P., and Mironova, A. A. (2016). Formation of Microstructures in Ti-Cr-V Alloys with High Hydrogen Sorption Capacity. *Chem. Met. Alloys* 9, 158–163. doi:10.30970/cma9.0347

Young, K., Ouchi, T., Nei, J., and Wang, L. (2016). Annealing Effects on Laves Phase-Related Body-Centered-Cubic Solid Solution Metal Hydride Alloys. *J. Alloys Compd.* 654, 216–225. doi:10.1016/j.jallcom.2015.09.010

Yu, X. B., Wu, Z., Xia, B. J., and Xu, N. X. (2005). Improvement of Activation Performance of the Quenched Ti-V-Based BCC Phase Alloys. *J. Alloys Compd.* 386, 258–260. doi:10.1016/j.jallcom.2004.05.014

Conflict of Interest: The authors declare that the research was conducted in the absence of any commercial or financial relationships that could be construed as a potential conflict of interest.

Publisher's Note: All claims expressed in this article are solely those of the authors and do not necessarily represent those of their affiliated organizations, or those of the publisher, the editors, and the reviewers. Any product that may be evaluated in this article, or claim that may be made by its manufacturer, is not guaranteed or endorsed by the publisher.